Peña-Bahamonde, J., San Miguel, V., Nguyen, H. N., Ozisik, R., Rodrigues, D. F. & Cabanelas, J. C. (2017): Functionalization of reduced graphene oxide with polysulfone brushes enhance antibacterial properties and reduce human cytotoxicity. *Carbon*, 111, pp. 258-268.

DOI: 10.1016/j.carbon.2016.10.005

# Functionalization of reduced graphene oxide with polysulfone brushes enhance antibacterial properties and reduce human cytotoxicity

Janire Pe˜na-Bahamonde [a], Ver´onica San Miguel [a], Hang N. Nguyen [b], Rahmi Ozisik [c], Debora F. Rodrigues [b, **], Juan Carlos Cabanelas [a, *]

A B S T R A C T

The present study reports two routes to modify reduced graphene oxide (rGO) nanosheets with poly-sulfone (PSU) brushes via nitrene chemistry. The PSU polymer is bonded to rGO at the extremity (rGO-PSU end) and at the middle of the PSU chain (rGO-PSU mid). The resulting rGO-PSU synthetic products are carefully characterized by Raman and FTIR spectroscopy, XPS, TEM, and thermogravimetric analysis, evidencing the successful grafting of PSU onto rGO surfaces. The long-term stability of these nanosheets is also determined in common solvents. The antibacterial properties of polymer-functionalized rGO against the planktonic *Bacilus subtilis* and *Escherichia coli* are also investigated. It is established that the antimicrobial properties of these nanocomposites are due to the production of reactive oxygen species. The results also demonstrate that rGO-PSU mid presents better antimicrobial properties due to shorter polymer chains, which improves the contact of the microorganisms with the graphene surface.

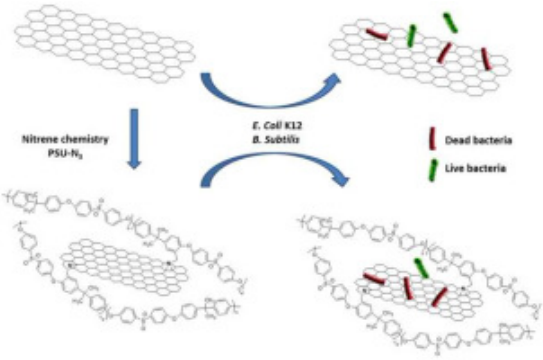


## 1. Introduction

The development and design of nanocomposites for application in diverse fields, such as materials science, nanotechnology, and biology have received considerable attention in the past years [1–4]. This interest comes from the potential synthesis of advanced functional materials with new, additional, or enhanced properties than their individual components. In particular, there is a widespread interest in incorporating nanomaterials into polymer matrices to create biocompatible polymeric membranes or to fabricate films for biomedical devices with antimicrobial properties [5–8]. Therein lies the special relevance to study the physicochemical and biocompatibility of reduced graphene oxide (rGO) in polymers.

Reduced graphene oxide is of particular interest, since functional groups on its surface enhance its solubility in organic solvents and remarkably facilitate surface modification with organic molecules or polymers [9]. The grafting of polymer brushes is of particular interest, because it improves the dispersion state and the polymer/graphene interfacial adhesion with the subsequent increase in both modulus and strength of the material [10]. During the nanocomposite synthesis, both the rGO/polymer ratio and the molecular weight of the graft polymer play an important role regarding rGO dispersion. This is because the behavior of polymer brushes is strongly determined by the polymer chain conformation. The grafting density and the critical spacing between two neighboring chains determine the brush regime, i.e. mushroom, crossover, and brush-like regimes. Depending on the conformation of the grafted polymer chain, the interactions with a polymer matrix may be improved [9,11].

Polysulfones (PSUs) are high-performance engineering thermoplastics that exhibit good chemical inertness, oxidative resistance, thermal, and hydrolytic stability, as well as high mechanical strength [12]. Additionally, PSUs may be easily processed as a film, and therefore, they are good candidates for many applications, such as gas separation, hemodialysis, nano/ultra-filtration, adhesives for metal-to-metal bonds, membranes for fuel cells, drug delivery or matrices for fiber-reinforced composites [7,13–15]. The incorpora-tion of non-functionalized rGO to polysulfones enhances their structural properties, hydrophilicity, chemical stability, or anti-fouling properties [16]. In addition, many studies have

* Corresponding author.
** Corresponding author.
*E-mail addresses:* dfrigirodrigues@uh.edu (D.F. Rodrigues), caba@ing.uc3m.es (J.C. Cabanelas).

[a] *Department of Materials Science and Engineering and Chemical Engineering, University Carlos III of Madrid, (IAAB), 28911 Leganés, Madrid, Spain*
[b] *Department of Civil and Environmental Engineering, University of Houston, 77204-4003 Houston, TX, USA*
[c] *Department of Material Science and Engineering Rensselaer Polytechnic Institute, 12180 Troy, NY, USA*

demonstrated that nanocomposites based on rGO [17–22] are good candidates for biomedical and environmental applications due to the antibacterial properties of graphene [5,18,19,23,24]. Nevertheless, to the best of our knowledge, grafting of polysulfone onto rGO has not been reported yet. Additionally, as shown in a recent review [17] there is a clear lack of knowledge about the influence caused by the grafting of polymer brushes on the antibacterial behavior and toxicity of graphene. The evident interest on enhancing the dispersion state, interfacial adhesion, and mechanical properties should not be reached at the expenses of the requirements for environmental and biomedicine applications. Therefore, the pre-sent work reports for the first time the functionalization of rGO with PSU chains through two different synthetic routes, and ana-lyzes how this surface modification affects the potential for bio-related applications through toxicity and biocompatibility tests. There are two main different approaches for anchoring polymer brushes to surfaces. The first one involves growing the polymer chain from the surface, i.e. "grafting from" method; and the second approach attaches a preformed polymer chain, i.e., "grafting to" method, by means of different mechanisms, such as ATRP [25–27], RAFT [28,29], click chemistry [30–33] or nitrene chemistry [33–36].

In this work, we apply nitrene chemistry to covalently graft PSU to rGO. The nitrenes are intermediates that can be generated from azide groups, either through thermolysis or irradiation. These highly reactive intermediates can be used to covalently modify rGO via the $(2 + 1)$ cycloaddition to the $\pi$-electron system of graphene [33,37,38]. Based on this approach, PSU was functionalized with azide, prior to grafting onto rGO, following known synthetic routes [39]. The procedures employed in the current work allowed to control the grafting density of PSU and to obtain polymer chains with extended conformation. Herein, we compare the extension and characteristics of the grafting and the solution properties of PSU end-linked and PSU mid-linked rGO. Varying concentrations of rGO modified with different polysulfone brushes were investigated to determine the effects of grafting of the polymer, as well as the concentration of modified nanosheets that leads to the most toxic concentrations against bacterial planktonic cells. We further evaluate their suitability as an antimicrobial agent for potential application in biomedical and industrial fields without any harm to human cells.

The results showed a successful modification of rGO with polysulfone brushes with a controlled anchoring point. The antimicrobial properties against *E. coli* K12 and *B. subtilis* showed that rGO-PSU mid and rGO-PSU end possess enhanced antimicrobial properties with respect to pristine rGO, however rGO-PSU mid was more effective in inactivating microorganisms than rGO-PSU end. These promising results open an opportunity to design rGO-PSU homopolymer nanocomposites with improved interfacial adhesion between graphene and the PSU matrix, maintaining the antimicrobial behavior and reducing cytotoxicity.

## 2. Experimental section

Graphene oxide (GO) was synthesized from natural graphite powder (Alfa Aesar, universal grade, ~200 mesh, 99.9995% purity) using a modified Brodie's method [40]. GO was subsequently reduced by thermal treatment to get reduced graphene oxide (rGO). Thermal reduction was carried out in an oven heated from room temperature to 500 °C at 5 °C·min$^{-1}$ in the presence of a $N_2$/$H_2$ (95/5%) gas mixture. Sodium azide (99%), chloroethyl isocyanate, chlorotrimethylsilane (98%), paraformaldehyde (95%), tin (IV) chloride (99%), *N,N*-dimethylformamide (DMF), *N*-methyl pyrrolidone (NMP), and anhydrous dichloromethane were purchased from Sigma-Aldrich and were used as received. A commercial PSU polymer (Mw ~35,000 g mol$^{-1}$, Mn~16,000 g mol$^{-1}$) was also supplied by Sigma Aldrich. The characterization is shown in the supporting information.

### 2.1. Grafting of PSU onto rGO

#### 2.1.1. Chloromethylation of PSU

Chloromethylation of PSU is the first stage before azidation. This step was performed by two different routes to obtain two distinct rGO modifications. The first route involved modifying graphene with anchoring points at the end of the polymer chain (rGO-PSU end); while the second method led to randomly linking rGO along the PSU chain (RGO-PSU mid). Both chloromethylation and subsequent azidation of PSU were confirmed by NMR and FTIR.

Modification of PSU at the end of the polymer chain (PSU end) is shown in Fig. 1. Chloromethylation of PSU was carried out in a vacuum line with a schlenk reactor. Then, PSU (5 g) was dissolved in 100 mL of anhydrous dichloromethane under nitrogen atmosphere. Chloromethyl isocyanate was added in stoichiometric amounts and the mixture was stirred for 24 h at room temperature. At the end of this period, the solution was precipitated in methanol and washed several times with methanol. The polymer (PSU–Cl) was then filtered and vacuum dried at 120 °C for 24 h.

The chloromethylation of the PSU along the polymer chain (PSU mid) was performed by reaction of chlorotrimethylsilane with PSU, as reported elsewhere [41], and is presented in Fig. 2. Some procedural modifications were introduced in order to achieve around one chloromethyl unit per PSU chain. Typical experimental conditions were as follows: PSU (5 g) was dissolved in 250 mL of chloroform. Paraformaldehyde (1.7 g) and tin (IV) chloride (0.07 mL) were added and the mixture was stirred until complete dissolution. Then, 7.16 mL of chlorotrimethylsilane was added dropwise. The solution was stirred for 5 h at 55 °C. The chloromethylated polysulfone (PSU–Cl) obtained was precipitated into methanol, washed several times, and then dried in a vacuum oven for one day at 120 °C. Cloromethylation degree was determined by NMR from Eq. (1):

$$\mathrm{CD}(\%) = \left(\frac{3\mathrm{A}(\mathrm{CH_2}-\mathrm{Cl})}{\mathrm{A}(\mathrm{CH_3})}\right) \times 100 \qquad (1)$$

where A($CH_2$–Cl) and A($CH_3$) are the integral areas of the hydrogens of methylene and methyl groups peaks, respectively, to confirm the monosubstitution of the polymer chain.

#### 2.1.2. Azidation of PSU

For both chloromethylated polysulfones, the same reaction procedure was used. PSU-Cl (1 g) was dissolved in 15 mL of DMF in a round-bottom flask, after which, sodium azide (200 mg) was added to the solution, and stirred for 24 h at 60 °C. The reaction mixture was then concentrated and precipitated with a methanol/water mixture (1:1, v/v). The product (PSU–$N_3$) was vacuum dried for 24 h at 100 °C.

#### 2.1.3. Surface functionalization of rGO nanosheets

Reaction of rGO with azide-terminal compounds has been described in literature extensively [36]. Nitrene chemistry was used for PSU-$N_3$ grafting to graphene in anhydrous NMP via aziridine bridge. rGO nanosheets (500 mg) were dispersed in NMP and sonicated for 1 h to create a homogeneous dispersion. One gram of PSU-$N_3$ was then dissolved with continuous stirring and the reac-tion mixture was heated to 160 °C and maintained for 48 h under nitrogen atmosphere. The reaction mixture was cooled down to room temperature, filtered, and washed several times with dichloromethane to remove unreacted PSU-$N_3$. The products (rGO- PSU mid and rGO-PSU end) were vacuum dried for 48 h at 100 °C.

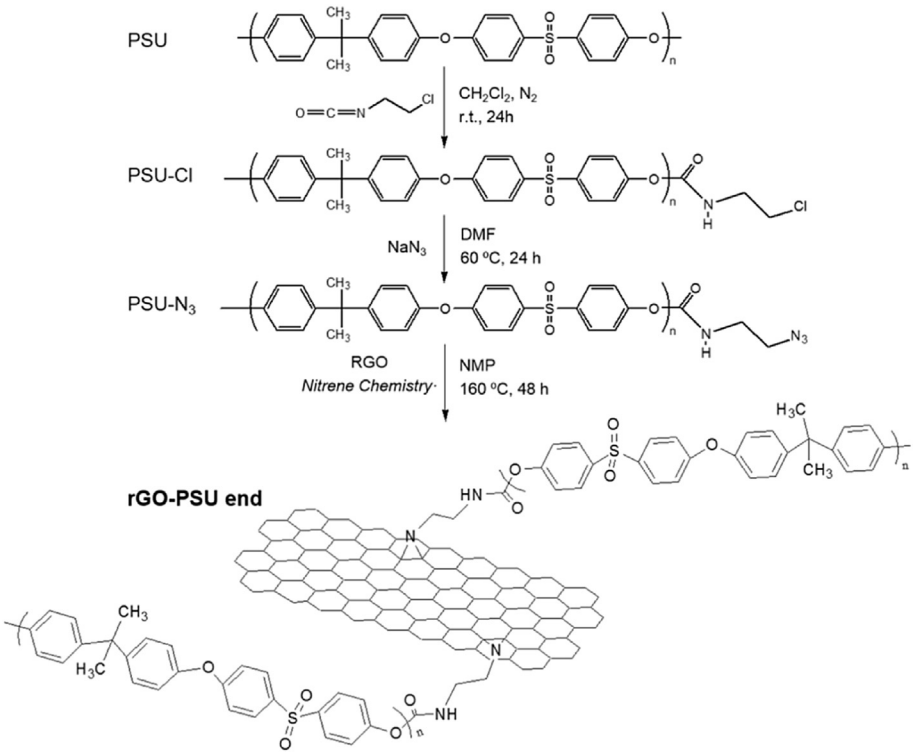


**Fig. 1.** Overall process for modification of rGO with functionalized polysulfone at the end of the polymer chain (PSU end).

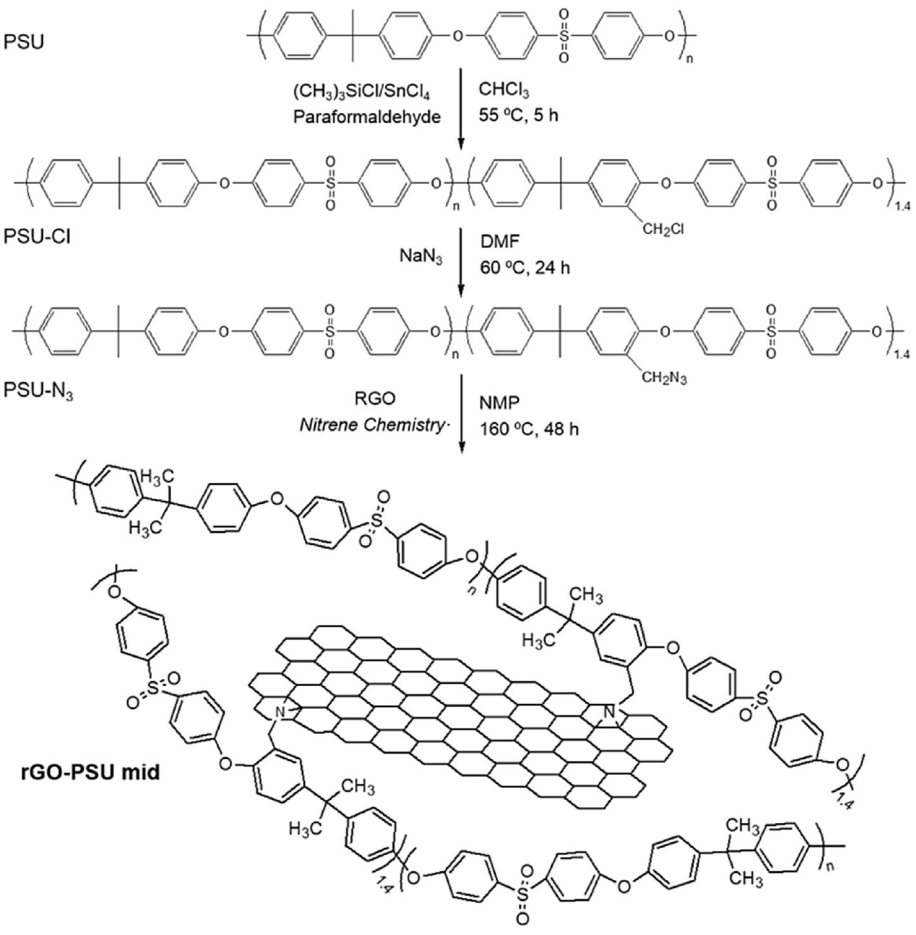


**Fig. 2.** Overall process for modification of rGO with functionalized polysulfone along the polymer chain (PSU mid).

## 3. Characterization techniques

The $^{1}H$ NMR measurements were recorded on a Bruker DPX 300 MHz spectrometer at room temperature using deuterated chloroform as solvent and tetramethylsilane (TMS) as an internal standard. Thermogravimetric analysis (TGA, Perkin Elmer STA 6000) was performed from 50 to 900 °C at 10 °C·min$^{-1}$ under nitrogen flow to study the chemisorption of the anchored polymer. Fourier transform infrared spectroscopy (FTIR, Perkin Elmer GX 2000) was analyzed in the medium range (4000–400 cm$^{-1}$) to test the functionalization of PSU and rGO-PSU nanocomposites. Ten scans were collected at 4 cm$^{-1}$ resolution. Attenuated diffusive reflectance (ATR) technique was employed to analyze rGO and modified rGO samples. Spectra were collected at 256 scans with a resolution of 4 cm$^{-1}$ on a Vector 22 apparatus. Powder X-ray diffraction (XRD, Philips X'pert Pro X-ray diffractometer) was employed to obtain the interlayer space on graphite and GO. The Cu Kα radiation was used ($\lambda = 1.54$ Å) at a scanning rate of 0.020° per second and from 5 to 40° in 2θ. The voltage was set to 40 kV, and the current to 40 mA. Raman spectroscopy (Renishaw Confocal Raman Microscope) was carried out with a 514.5 nm Ar laser excitation. For each sample, several spectra were recorded in different places on the sample in order to verify its homogeneity. X-ray photoelectron spectroscopy (XPS, Physical Electronics PHI 700 Auger scanning probe) was performed employing a monochromated Al Kα X-ray source (1486.6 eV). High-resolution spectra were acquired with a pass energy of 23.5 eV, an energy step size of 0.2 eV, and a time step of 50 ms. For microstructural, analytical information, and antimicrobial assays, nanoparticles were characterized by high resolution scanning electron microscopy (SEM, Nova NanoSEM 230) and high resolution transmission electron microscopy (TEM, JEOL 2200FS). TEM samples were prepared by placing a drop of a diluted dispersion in absolute ethanol onto copper grids and drying them in air.

### 3.1. Antibacterial and toxicity evaluation

#### 3.1.1. Bacterial suspension preparation

The bacterial strains utilized in the present study were *Escherichia coli* K12 and *Bacillus subtilis*. For all microorganisms, tryptic soy broth (TSB) was used as growth medium (Oxoid Ltd., Basingstone, Hampshire, England). A single isolated colony was inoculated in 5 mL TSB to grow overnight at 35 °C. The grown bacterial culture was centrifuged at 10,000 rpm for 5 min, and the bacterial pellet was washed once and resuspended in phosphate buffer solution (PBS). The optical density (OD) of the suspension was adjusted to 0.2 at 600 nm, which corresponds to a concentration of $10^6$ colony forming units (CFU) per mL. The concentration was determined based on the plate count method for each bacterium using tryptone soy agar (TSA, Oxoid Ltd.).

#### 3.1.2. Toxicity of nanomaterials

The planktonic Gram-positive and Gram-negative bacterial interactions with polymer-modified rGO nanocomposites were evaluated via the following methods: optical density (OD) growth measurements, plate count method, and scanning electron microscopy (SEM), as previously described [8,18,21].

For this investigation, stock solutions for all nanocomposites with a concentration of 1000 ppm were prepared. Aliquots of 100 μL of bacterial suspension at 0.2 $OD_{600}$ in PBS were placed in a 96-well plate (Greiner bio-one) and varying amounts of nanoparticles (rGO, rGO-PSU mid, or rGO-PSU end) were added into the wells to obtain different concentrations (10, 50, 100, 200, and 500 ppm). Three replicates of each nanomaterial concentration and controls were done. Blanks were prepared with the nanocomposites and sterile distilled water. Similarly, negative controls aiming to determine contamination during the experiments were carried out with PBS only. The 96-well plate was incubated for 3 h at 35 °C to allow bacteria to be exposed to the nanomaterials.

For the optical density growth method, aliquots of 20 μL of the bacterial–nanocomposite suspensions were transferred after 3 h incubation to a new 96-well plate containing 200 μL of Tryptic Soy Broth media (TSB). The plate was incubated for 10 h to allow bacterial growth. The optical density was recorded every 30 min using a Synergy MX Microtiter plate reader (Biotek). The growth curves were generated by plotting the average OD values versus growth time. Statistical analysis (two-sided *t*-test, 95% confidence interval) was performed to determine whether the OD values of the nanomaterials were statistically different than the OD values of the control.

The plate count method was performed to confirm the toxicity of the nanomaterials. Serial dilutions of the cells incubated for 3 h with the nanomaterial solutions were plated in Tryptic Soy Agar (TSA) by spread plate method. Every TSA plate was incubated overnight at 35 °C and the colony forming units (CFU) in each plate was counted. The results were expressed in (CFU·mL$^{-1}$) versus concentrations of each material.

All incubated stock solutions were centrifuged to collect the pellets and fix cells before SEM analysis [42]. The fixation of cells was carried out by treatment of samples with 2% glutaraldehyde for 30 min at room temperature, followed by incubation for 1 h at 4 °C and staining with 1% Osmium Tetroxide solution for 30 min. A post fixation was performed through a series of washing with 0.05 M sodium cacodylate buffer. Afterwards, the dehydration process was carried out using progressive series of ethanol concentrations from 25 to 100%. Propylene oxide was added to each sample to suspend the cells. Finally, one drop of the suspension was laid over a clean glass slide and allowed to dry at room temperature overnight before SEM imaging.

#### 3.1.3. Production of reactive oxygen species (ROS)

Quantification of thiol concentration in glutathione (GSH) molecules was previously described as an indirect method to measure reactive oxygen species (ROS) production by nanomaterials [43]. All the samples: rGO, PSU, rGO-PSU mid, and rGO-PSU end were investigated for ROS production in triplicate at 500 ppm. Briefly, 0.4 mM GSH was allowed to react for 2 h at room temperature with samples at 500 ppm, negative controls with non-oxidative agent, and positive controls containing hydrogen peroxide. After which, 100 mM Ellman's reagent was introduced into each tube and allowed to react for 10 min. All particles were removed by using a 0.2 μm syringe filter (Corning, U.S.A.). The filtrate was read at 412 nm using Synergy MX Microtiter plate reader to measure the loss of thiols. The results were expressed as the loss of GSH and represented by Eq. (2).

$$\text{GSH loss } (\%) = \frac{(\text{Absorbance negative control} - \text{Absorbance sample})}{\text{Absorbance negative control}} \times 100$$

*3.1.4. Nanocomposite toxicity to human cells*

Human cytotoxicity of the nanocomposites were investigated with 500 ppm with all the nanomaterials produced in this study, following a procedure previously described [18,44]. In the current work, immortalized human corneal epithelial cell line (hTCEpi) obtained from Prof. Alison M McDermott was used to investigate the cytotoxicity of the nanocomposites. The hTCEpi cells were cultured at 37 °C in 5% $CO_2$ humidified incubator (NuAire, U.S.A) for 48 h with KBM-2 complete media (Lonza, U.S.A Catalog# CC-3107). Cell culture with a density of $30 \times 10^4$ cells per mL was harvested after 48 h at the passage 54 and seeded to a 96-well plate (Falcon, U.S.A). The cells were further incubated at 37 °C with 5% $CO_2$ humidified air incubator for 24 h. After rinsing 3 times with PBS, 100 μL of nanomaterials, negative control (PBS), and positive control (0.02% of benzalkonium chloride, BAC) were added to the cells containing 100 μL growth medium in each well. The plate was incubated for another 24 h. All experiments were performed in triplicate. After 24 h incubation with nanomaterials, all supernatant was aspirated from the wells and the plate was rinsed again 3 times. The detection reagent from the assay kit and medium were added to the wells with a 1:5 ratio. After 3 h incubation, the plate was read at 490 nm with the use of micro-plate reader FLUOstar Omega (BMG Labtech, Germany). All the results were expressed in terms of percentage of living cells in comparison to the negative control, as presented in Eq. (3).

$$\text{Live cells } (\%) = \frac{\text{Absorbance of samples or positive control}}{\text{Absorbance of negative control}} \times 100\% \quad (3)$$

## 4. Results and discussion

*4.1. PSU-$N_3$ synthesis*

The general strategies for the preparation of graphene nanosheets functionalized with PSU brushes were presented in Figs. 1 and 2. Both processes involve first the chloromethylation of polysulfone (PSU−Cl). The chloromethyl units of the resulting polymer were converted to azide groups by a simple substitution reaction to give PSU-$N_3$. Finally, rGO modification with functionalized PSU polymer was carried out by nitrene chemistry. The success of chloromethylation and azidation reactions was confirmed by NMR and FTIR analyses.

The chloromethylation degree was estimated from the integration ratio of the $^1$H NMR signal of $-CH_2Cl$ protons located at 4.6 ppm to that of the six protons of the methyl groups appearing at 1.7 ppm [12]. Under the experimental conditions selected in this work, 5 h reaction time and 1:180 PSU/chlorotrimethylsilane molar ratio, just one in 25 PSU repetitive units were functionalized. Taking into account the molecular weight of the PSU, this corresponds to an average number of 1.4 anchoring points per chain, avoiding the possibility to obtain a cross-linked structure. NMR spectra also confirmed, under these synthetic conditions, that there was never more than one chloromethyl group attached per benzene ring [45].

After treatment with sodium azide, the signals corresponding to methylene protons (-$CH_2N_3$) shifted from 4.6 to 4.3 ppm for PSU mid, which indicated successful azidation. Degree of azidation of the functionalized polymers was determined according to the integrated intensity ratio of methylene protons to that of the six protons of the methyl groups (1.7 ppm). The conversion of the chloromethyl group into the azide functional group was nearly complete.

*4.2. Synthesis and characterization of PSU functionalized graphene*

The successful synthesis of GO and rGO was confirmed with X-ray diffraction as shown in Fig. S1. The strong diffraction peak at $2\theta = 26^\circ$ in pristine graphite corresponds to the d(002) spacing (0.337 nm) of graphite carbon in an ordered structure. The GO diffraction pattern showed a peak at $2\theta = 15.8^\circ$, r e flecting a much larger interlayer spacing, which was 0.598 nm. This reveals the presence of oxygenated functional groups after oxidation. These functional groups cause a more loosely stacking of graphene oxide sheets than pristine graphite. The strong peak of GO vanished in the rGO pattern, which in turn showed a broad peak in the range of 20.0°−27.2°, indicating that some aggregation occurred during thermal reduction. The broad diffraction peak of rGO indicates also poor ordering of the sheets along the stacking direction, which implies the sample was comprised mainly by a few layers of rGO with a disordered packaging.

Raman spectroscopy allows the distinction between ordered and disordered structures of carbonaceous materials [46]. Raman spectra of pristine graphite, GO, and rGO are shown in Fig. S2. Spectra of PSU and modified graphene with functionalized polymers (rGO-PSU mid and rGO-PSU end) are also included on the graph and will be discussed later. As expected, the pristine graphite displayed a prominent G band centered at 1585 $cm^{-1}$, which corresponds to the first-order scattering of the $E_{2g}$ mode and is associated with the vibration of $sp^2$ carbon atoms. The Raman spectrum of GO presented a strong D band at 1358 $cm^{-1}$ and also a strong G band at 1589 $cm^{-1}$. The D band belongs to the activation in the first order scattering process of disordered $sp^2$-bonded carbon atoms [47]. The widened and shifted G band is related to the influence of defects and isolated double bonds; and therefore to a reduced distance between defects [48]. The rGO Raman spectrum displayed the G band at 1585 $cm^{-1}$ and the D band at 1355 $cm^{-1}$. The comparison of the intensity of the D and G bands may help to elucidate the extent of carbon-containing defects, and therefore, to derive information about the disordered and ordered crystal structures of carbon. The value of the intensities of D and G bands I(D)/I(G) (peak height ratio) reached a value of about 0.98 for GO due to the severe oxidation that causes many disorders in the hexagonal graphitic layers. After thermal reduction, the ratio was 0.92. Therefore, the degree of disorder in the structure does not significantly change within our experimental conditions.

The covalent attachment between graphene sheets and PSU chains was confirmed using FT-IR, TGA, Raman spectroscopy, and XPS. Surface morphology of the modified graphene nanosheets was also investigated by SEM and TEM techniques. The FTIR comparative analysis of rGO and polymer-modified graphene samples (rGO-PSU mid and rGO-PSU end) is shown in Fig. 3b. In both rGO-PSU nanocomposites, it can be clearly observed the presence of characteristic vibronic bands corresponding to the PSU backbone, such as aromatic C═C asymmetric and symmetric stretching (1552, 1486, and 1169 $cm^{-1}$), O═S═O symmetric stretching (1151 $cm^{-1}$) or C−O−C asymmetric stretching (1242 $cm^{-1}$), confirming successful surface modification of rGO.

Raman spectra of rGO-PSU mid and rGO-PSU end samples are shown in Figs. S2e and S2f, respectively. In these nanocomposites, the G band is shifted and its intensity is increased, due to the contribution of the highly aromatic PSU grafted chains. As shown in Fig. S2a, the PSU Raman spectrum presents an absorption band at around 1540 $cm^{-1}$ corresponding to the C atoms of the phenylene units. This band coincides with the G band of the rGO, and so it contributes to the apparent decrease in the I(D)/I(G) ratio, making unfeasible to subtract the contribution of the $sp^2$ bonds from PSU.

Thermogravimetric curves from the reduced graphene oxide, PSU, and the two modified graphene samples are shown in Fig. S3.

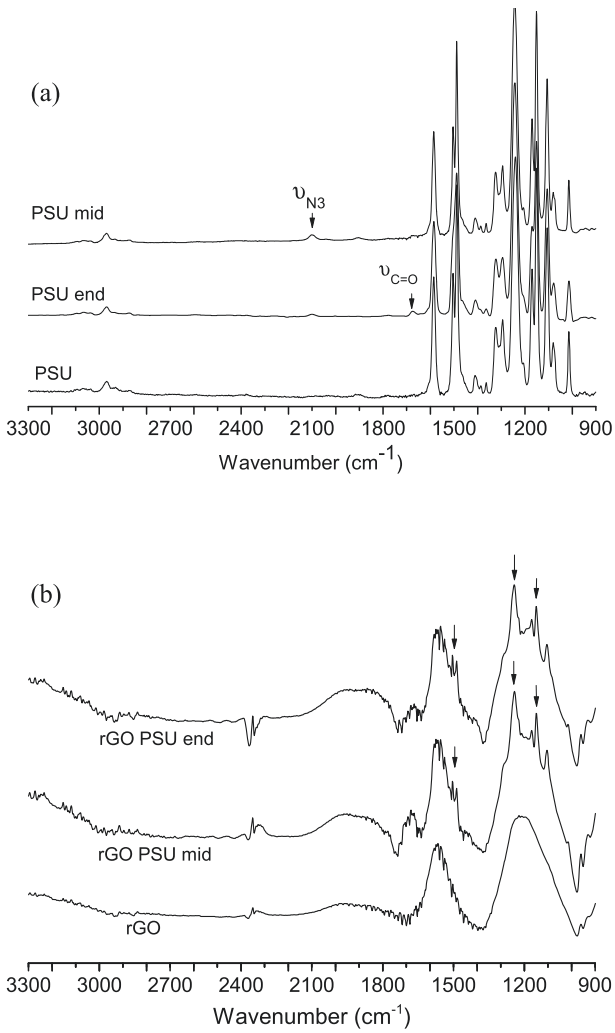


**Fig. 3.** FTIR spectra of (a) polysulfone (PSU) and functionalized PSU along the polymer chain (PSU mid) and at the end of the chain (PSU end); (b) rGO and modified graphene with PSU brushes along the polymer chain (rGO-PSU mid) and at the end of the chain (rGO-PSU end). Arrows focus on the main PSU vibronic bands.

The rGO presented 18% weight loss in the whole range between 100 and 800 °C. The mass loss at high temperature is attributed to the pyrolysis of labile oxygen-containing groups, generating CO, $CO_2$, and steam. In contrast, polymer branched samples exhibited an additional mass loss step at around 450 °C, which arises from the PSU organic backbone grafted to the rGO, and roughly coincides with the onset of the main degradation step of PSU. The number of grafted PSU chains per carbon atom and the surface grafting density may be calculated according to Eqs. (4) and (5), respectively [49].

$$\text{Density}_{\text{chain}} = \frac{M_C W_P}{M_P W_C} \quad (\text{chains per C}) \tag{4}$$

$$\text{Density}_{\text{area}} = \frac{M_C W_p 10^8}{M_p W_C A_b} \left(\text{chains per } \mu m^2\right) \tag{5}$$

where, $M_C$ is the relative molar mass of carbon (12 g $mol^{-1}$) and $M_P$ is the average molecular weight of grafted polymer: 16,000 g $mol^{-1}$ for rGO-PSU end and 8000 g $mol^{-1}$ for rGO-PSU mid, since the anchoring point has been considered randomly situated along the polymer chain. $W_C$ and $W_P$ are the weight fractions of the rGO backbone and the grafted polymer, respectively, determined from the TGA curves. $A_b$ corresponds to the benzene ring area in graphene (5.24 $Å^2$). The grafting densities obtained are presented in Table 1. The weight loss of rGO-PSU end sample was 32% in the range between 100 and 800 °C, because it includes, along with the rGO degradation, the thermal degradation of the grafted PSU. After correction, considering the rGO weight loss in the same range, this loss corresponds to functionalization with approximately one polymer chain per 2800 carbon atoms on the graphene basal planes, or 0.67 chains per area (in $\mu m^2$). rGO-PSU mid presented a higher grafting density, one chain per about 1600 carbon atoms, since each anchoring point generates two polymer chains, but with smaller length. The functionalization degrees of rGO were closed to those previously reported for functionalized CNTs and rGO nanosheets with polymer brushes [49], r e flecting the efficiency of nitrene functionalization.

X-ray photoelectron spectroscopy (XPS) analysis was used to elucidate the surface elemental composition of different specimens. The carbon 1s XPS spectra can be resolved by curve-fitting into several peaks with attributable binding energies [50–52]. The results are shown in Fig. 4. The C 1s XPS spectrum of GO clearly indicated a high degree of oxidation corresponding to carbon atoms in different functional groups: the non-oxygenated ring C–C ( a broad band belonging to a mixture of $sp^2$ and $sp^3$ carbons)(284.8 eV), the C–O (286.7 eV), and the carbonyl C=O (287.5 eV). Comparison of the GO and rGO XPS spectra (Fig. 4a and b) evidenced a considerable deoxygenation during the reduction process as revealed by the lower contribution of oxygenated peaks in the rGO, as well as the increased intensity of the C–C peak at 284.8 eV, that account for around 70% of carbon atoms. After nitrene chemistry reaction, the C 1s XPS spectra of modified rGO samples did not require additional peaks to reach good fittings, although the relative intensity, width, and energy of the peaks showed several differences. Grafting of the PSU should be manifested by the presence of additional C–S (sulfone group) and C–N (PSU functionalization) bonds, but their binding energies present a significant overlap with the one of the C–O emission band [50–52]. Moreover, the contribution of the grafted PSU to the XPS spectra will come mainly from the C–C (and C–H) bonds of the PSU backbone, which represents more than 75% of carbon bonded atoms, and the contribution of C–S and C–N has to be very low. Therefore, we considered the C–S and C–N bonds embedded in the C–O band, making unfeasible the quantification of the grafting. The best deconvolution results are presented in Fig. 4c and d. The C–C/C–H band remains the most intense, and the C–O/C–S/C–N mixed band shows a remarkable broadening respect to the C–O band of rGO.

A relevant analysis to confirm PSU grafting into the graphene surface was obtained with XPS and deconvolution analysis of the N 1s peaks, at around 400 eV. The N 1s XPS spectra of rGO-PSU mid and rGO-PSU end (Fig. 4e) verify the existence of nitrogen-containing groups on graphene surface due to the inclusion of nitrogen in the aromatic structure of the rGO as an aziridine ring (C–N bond at 400,4 eV), as previously reported [53]. The peak broadens for rGO-PSU end because of the contribution of two C–N species to the N 1s peak, the aziridine ring and the urethane. In contrast, no N 1s signal was detected in rGO. N 1s spectra also confirmed the success in the nitrene chemistry route for grafting the PSU, as revealed by the complete absence of azide nitrogen characteristic peaks in the grafted PSUs.

Fig. 5 shows the TEM images of rGO and rGO modified nanosheets at high magnification. The edge of the flakes reveals the presence of multilayers between 6 and 9 nm thickness. PSU-modified graphene samples seem to show a lower agglomeration.

The success of the nitrene chemistry has been supported by FT-IR, Raman, TGA, XPS, and microscopy observations. Furthermore,

**Table 1**
Data obtained from TGA curves and Raman spectroscopy of rGO and modified rGO with functionalized polysulfone.

| Sample | TGA | | |
|---|---|---|---|
| | Weight loss (wt%)[a] | Density[b] (chains/$10^4$ C atoms) | Density[c] ($\times 10^{-4}$ chains/$\mu m^2$) |
| rGO | 18.3 | – | – |
| rGO-PSU end | 32.0 | 3.53 | 0.67 |
| rGO-PSU mid | 29.1 | 6.16 | 1.18 |

[a] Determined from 100 °C to 800 °C of TGA curves. Weight loss for rGO-PSU samples includes the thermal loss from both the polymer and the rGO. [b] Average number of PSU chains per 10,000 carbon atoms of graphene, calculated from Eq. (1).
[c] Average PSU chains density per area (in $\mu m^{-2}$) of graphene, determined from Eq. (2).

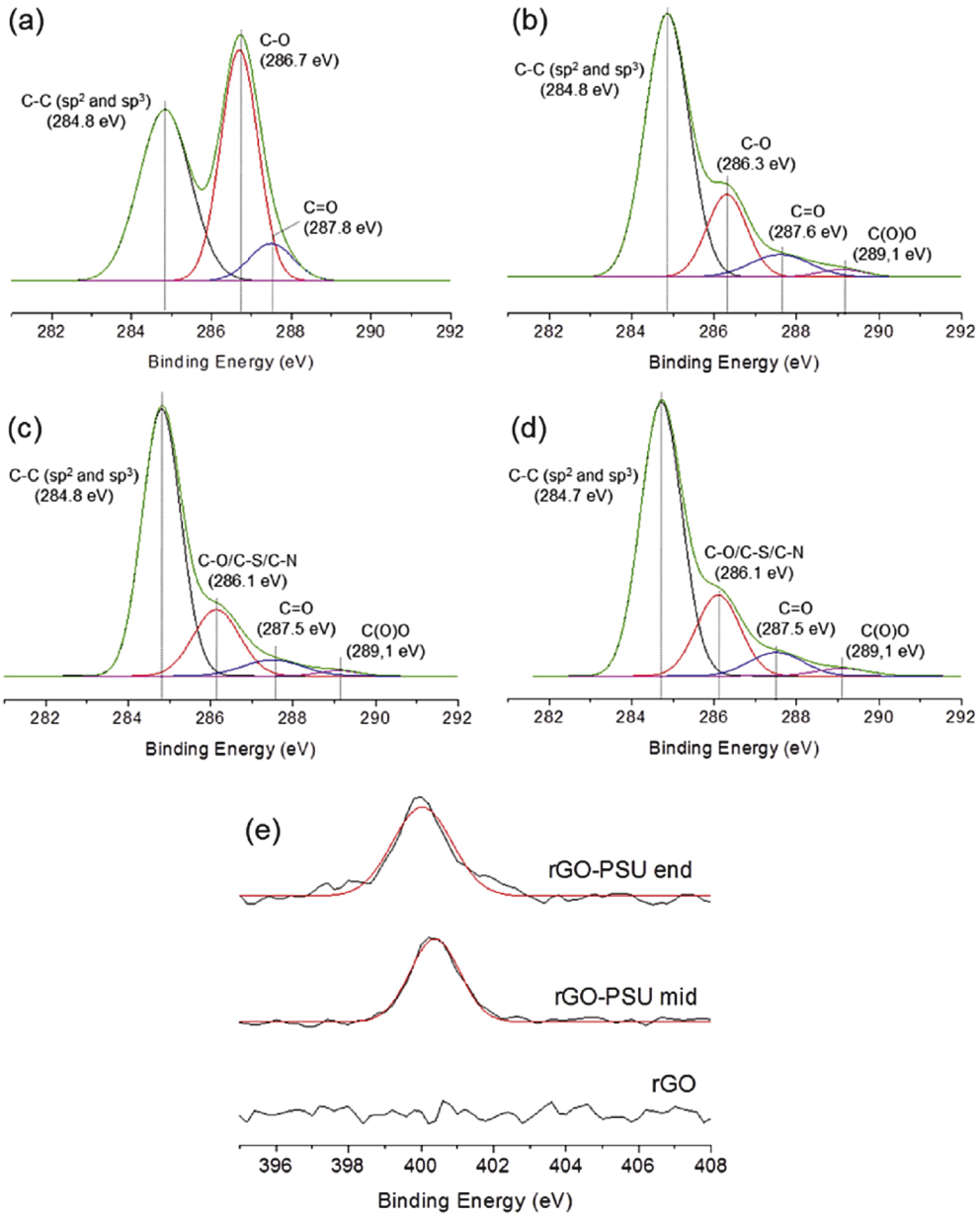


**Fig. 4.** a-d) XPS spectra of C 1s peak of: a) GO, b) rGO,c) rGO-PSU mid, d) rGO-PSU end e) XPS spectra of N 1s peak of: rGO, rGO-PSU mid and rGO-PSU end. (A colour version of this figure can be viewed online.)

the improvement of graphene dispersability after polymer modification of graphene was investigated in water and *N*-methylpyrrolidone (NMP), which are good solvents for PSU. The rGO-PSU nanosheets were sonicated in water or NMP at a concentration of 0.5 g $mL^{-1}$. Images of graphitic dispersions in both solvents are shown in Fig. S4. Dispersion stability of PSU-modified graphene samples in water was significantly lower (<5 min) than in NMP, in which the suspension remained stable for at least 5 h. This different dispersability is in agreement with the fact that water is a poor solvent and NMP is a good solvent for polysulfone. This result

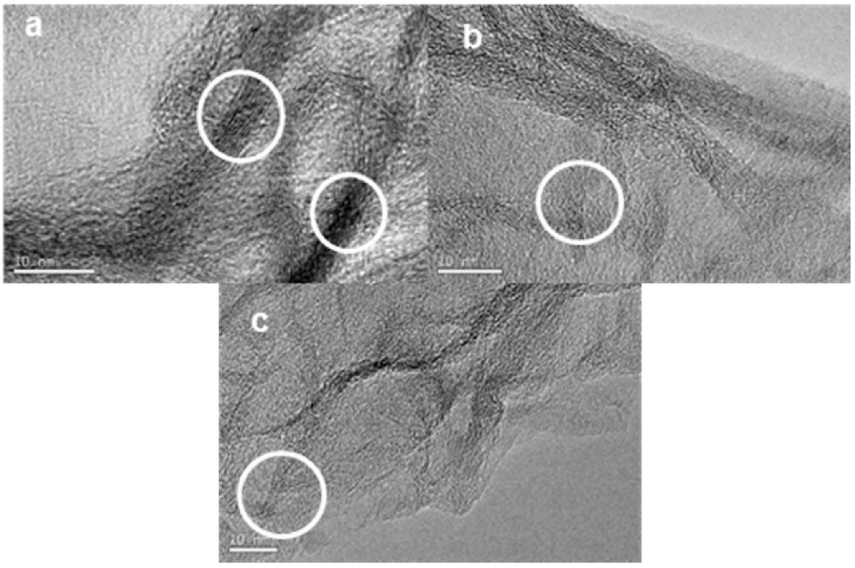


**Fig. 5.** TEM images at high magnification of (a) rGO; (b) rGO-PSU mid; (c) rGO-PSU end.

indicates that PSU modified graphene can be used as nano-reinforcement for polymer matrices.

### 4.3. Antimicrobial and cytoxicity of nanomaterials

The toxicity of the new nanocomposites to both Gram-positive and Gram-negative microorganisms was investigated at varying concentrations of polysulfone modified rGO (rGO-PSU mid and rGO-PSU end). The antimicrobial activity determined after 3 h of exposure to nanomaterials showed that *B. subtilis* is more sensitive than *E. coli* K12, as observed by the 90% and 40% cell inactivation at 500 ppm for rGO-PSU mid, respectively (Fig. 6a and b). This difference in the results between *E. coli* K12 and *B. subtilis* is attributed to the presence of an external cell membrane in the Gram-negative and absence of it in the Gram-positive bacteria [54]. This higher sensitivity of Gram-positive bacteria was previously observed by Carpio et al. [21]. The same inactivation trend was observed in the optical density results (Fig. S5). *E. coli* K12 exposed to 500 mg $L^{-1}$ for all the rGO materials presented reduced growth than the control samples having no rGO. Noticeably, the growth inhibition was 40%, 20%, and 20% for rGO-PSU mid, rGO-PSU end, and rGO, respectively. For *B. subtilis*, rGO-PSU mid was also the most toxic. The highest inactivation of *B. subtilis* was 90%, which was observed at 500 mg $L^{-1}$ with rGO-PSU mid, following 36, 48, 46%, and 51%, corresponding to 200, 100, 50, and 10 mg $L^{-1}$ rGO-PSU mid, respectively (Fig. S5b). For both *E. coli* and *B. subtilis*, PSU did not show any toxicity activity at any concentrations. In general, the modification of rGO with PSU improved the antibacterial properties of rGO, especially at the highest concentration tested (500 mg $L^{-1}$). Therefore, the results clearly show that rGO-PSU mid, which presents the lowest molecular weight brush, is more antimicrobial than rGO-PSU end. These results were observed for both *E. coli* K12 and *B. subtilis* (Fig. 6 and Fig. S5) and suggest that shorter polymer brushes allow better contact of the bacteria with the rGO surface. Consequently, molecular weight of the polymer (i.e. length of the brush) may influence the antimicrobial property of the nanocomposite. Further comparison of these results with previous studies available in the literature shows that reduced graphene oxide with polymer brush expressed higher antimicrobial activity than other nanocomposites (Table S1). This comparison also shows that the antimicrobial effect of rGO depends on the microorganisms and the type of nanocomposite.

To understand the mechanism of inactivation of these new nanocomposites, we investigated the production of reactive oxygen species (ROS). ROS was previously reported to be one of the inactivation mechanism of graphene-based nanomaterials [54]. A s

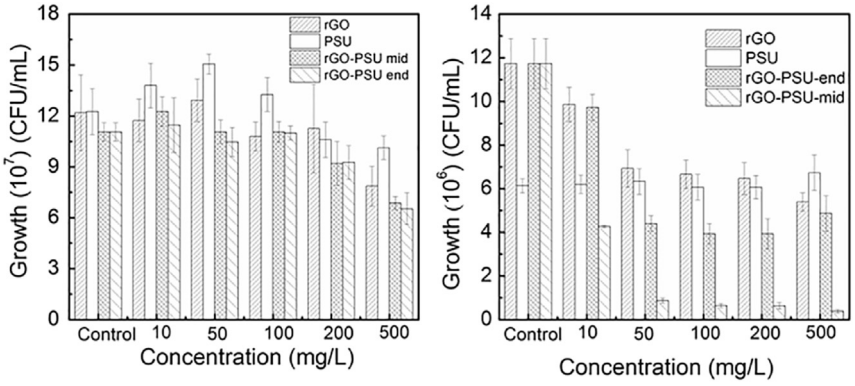


**Fig. 6.** Plate count results of (a) *E. coli* K12 and (b) *B. subtilis* after 3 h of exposure to nanomaterials at varying concentrations. The control sample contains only the bacteria and no nanomaterial.

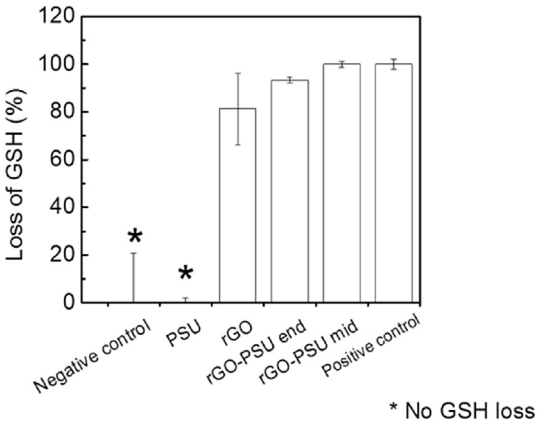


**Fig. 7.** Reactive oxygen species (ROS) activity of rGO nanocomposite samples at 500 ppm. Results are expressed as loss of glutathione (GHS).

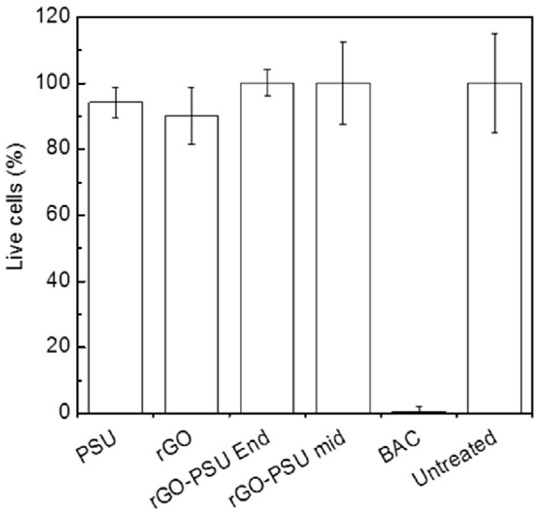


**Fig. 9.** Percentage of live hTCEpi cells after 24 h exposure to the nanomaterials at 500 ppm. BAC corresponds to cells inactivated with 0.02% of benzalkonium chloride (positive control). The untreated cells correspond to the negative control.

presented in Fig. 7, samples of rGO, rGO-PSU end, and rGO-PSU mid all resulted in significant loss of GSH. The results showed that GSH loss increased from 81% for rGO to 93% for rGO-PSU end and to 100% for rGO-PSU mid. These results of ROS correlate well with the microbial inactivation observed in Fig. 6 and Fig. S5, and corroborate previous reports about the antimicrobial activity of graphitic nanomaterials, which describe ROS as one of the most important microbial inactivation mechanisms [43]. Scanning electron microscopy (SEM) images of planktonic cells exposed to 500 ppm of nanomaterials are showed in Fig. 8. SEM images of the control cells and cell treated with PSU (Fig. 8a and b) revealed that the bacteria were intact, since their rod shape and cell integrity were maintained. In contrast, images of the rGO-PSU mid and rGO end interaction with the bacteria cells (Fig. 8c and d) pointed out that nanomaterial may be wrapping around the bacteria. These bacteria exhibited some deformation, which indicates cell damage. The observation of wrapping cells or embedding in large rGO-PSU aggregates are essential in antimicrobial behavior and was reported previously [43,55].

The promising properties of graphene based nanomaterials and their potential application in different fields have attracted the attention of diverse researchers and companies. It is essential, however, to design nanomaterials that are safe to the environment and to humans; and at the same time have properties attractive for diverse industries. PSU is commonly used for biomedical and water treatment applications [56,57]. In the current study, the grafting of PSU to rGO produced an antimicrobial nanocomposite that if incorporated in medical devices or filtration membranes could potentially reduce microbial contamination and prevent biofouling. The application of these rGO-PSU nanocomposites would, however, involve direct human exposure. Therefore, investigating the human cytotoxicity of these nanocomposites is necessary. In the current study, human hTCEpi cells were exposed to various samples at 500 ppm. These cell lines were used since corneal cells are well

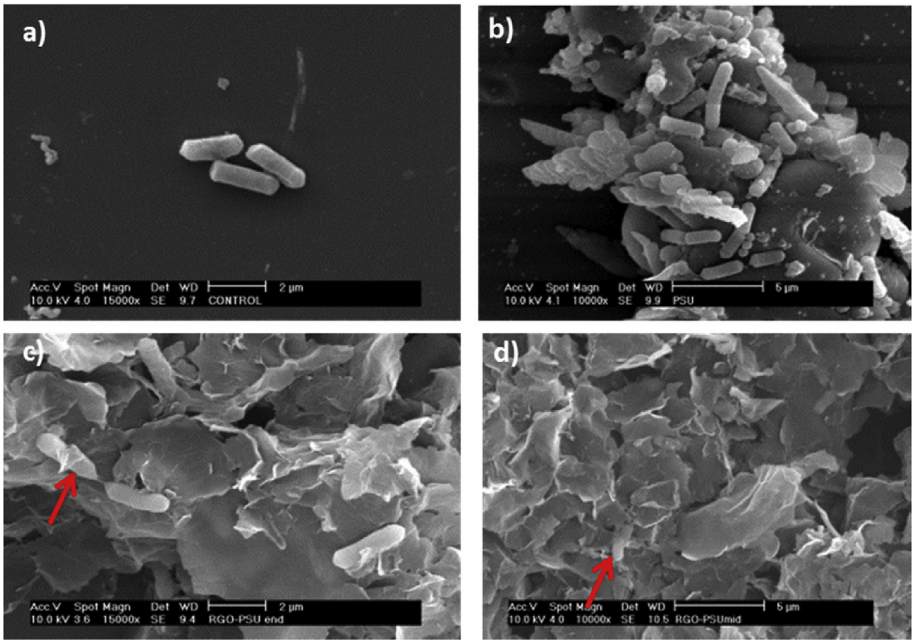


**Fig. 8.** SEM images of (a) *B. subtilis* control, (b) *B. subtilis* exposed to 500 ppm PSU, (c) *B. subtilis* exposed to 500 ppm rGO-PSU end, and (d) *B. subtilis* exposed to 500 ppm rGO-PSU mid. (A colour version of this figure can be viewed online.)

known to be extremely sensitive to chemicals and toxic materials. The exposure results showed no negative effects to the cells, since cells exposed to 500 ppm of nanocomposites for 24 h did not die (Fig. 9). These results suggest that the graphene nanocomposites developed in a current study can potentially be used in materials or devices that will have direct exposure to humans. Further studies, however, should be performed with other human cell lines and model animals to confirm these results.

## 5. Conclusions

In summary, we have successfully applied nitrene chemistry to functionalize PSU onto rGO sheets. The synthetic strategy presented in this work demonstrates that modified graphene nanosheets can be easily obtained in high yields. Additionally, the general strategy described here can be easily extended to synthesize other polymer-functionalized graphene materials. The resulting nanomaterials have suitable dispersability and processability in organic solvents; and present improved antimicrobial behavior compared to non-modified rGO. Results indicate that shorter and low molecular weight polysulfone brushes allow better interaction of rGO with microorganisms and, therefore, present higher antibacterial property than longer and high molecular weight PSU brushes. One of the mechanisms of microbial inactivation identified in the current study for these new nanocomposites is the production of reactive oxygen species. Investigation of the human cytotoxicity of these novel nanocomposites suggests that they can be safely used in applications involving human exposure.

## Acknowledgements

This work was financially supported by the Spanish Ministry of Economy and Competitiveness (MAT2014-57557-R), and partially supported by the U.S. National Science Foundation Career Award (NSF Award #104093). R.O. would like acknowledge support from U.S. National Science Foundation (CMMI-1538730 and DUE-CMMI-1538730/1003574). Janire Peña wants to acknowledge mobility grant from Carlos III University and Instituto Tecnológico de Química y Materiales "Alonso Barba". Authors acknowledge Dr. A. Esteban-Arranz for giving access to ATR equipment.

## References

[1] O.C. Compton, S.T. Nguyen, Graphene oxide, highly reduced graphene oxide, and graphene: versatile building blocks for carbon-based materials, Small 6 (2010) 711–723.
[2] S. Marchesan, M. Prato, Nanomaterials for (Nano)medicine, ACS Med. Chem. Lett. 4 (2013) 147–149.
[3] J. Du, H.-M. Cheng, The fabrication, properties, and uses of graphene/polymer composites, Macromol. Chem. Phys. 213 (2012) 1060–1077, http://dx.doi.org/10.1002/macp.
[4] J.H. and B.P. Gergely Keledi, Polymer nanocomposites: structure, interaction, and functionality, Nanoscale. 4 (n.d.) 1919–1938.
[5] K.C. Kemp, H. Seema, M. Saleh, N.H. Le, K. Mahesh, V. Chandraa, K.S. Ki, Environmental applications using graphene composites: water remediation and gas adsorption, Nanoscale 8 (2013) 3149–3171.
[6] H. Liu, L. Hou, W. Peng, Q. Zhang, X. Zhang, Fabrication and characterization of polyamide 6-functionalized graphene nanocomposite fiber, J. Mater. Sci. 47 (2012) 8052–8060.
[7] S. Kim, L. Chen, J.K. Johnson, E. Marand, Polysulfone and functionalized carbon nanotube mixed matrix membranes for gas separation: theory and experiment, J. Memb. Sci. 294 (2007) 147–158.
[8] I.E. Mejias Carpio, J.D. Mangadlao, H.N. Nguyen, R.C. Advincula, D.F. Rodrigues, Graphene oxide functionalized with ethylenediamine triacetic acid for heavy metal adsorption and anti-microbial applications, Carbon N. Y. 77 (2014) 289–301.
[9] O. Azzaroni, Polymer brushes here, there, and everywhere: recent advances in their practical applications and emerging opportunities in multiple research fields, J. Polym. Sci. Part A Polym. Chem. 50 (2012) 3225–3258.
[10] M. Cano, U. Khan, T. Sainsbury, A. O'Neill, Z. Wang, I.T. McGovern, W.K. Maser, A.M. Benito, J.N. Coleman, Improving the mechanical properties of graphene oxide based materials by covalent attachment of polymer chains, Carbon N. Y. 52 (2013) 363–371.
[11] S. Wang, B. Jing, Y. Zhu, Molecule motion at polymer brush interfaces from single-molecule experimental perspectives, J. Polym. Sci. Part B Polym. Phys. 52 (2014) 85–103.
[12] P.T. Mcgrail, Polyaromatics, polym, Int 41 (1996) 103–121.
[13] S.S. S´anchez, Phase-inversion method for incorporation of metal nanoparticles into carbon-nanotube/polymer composites, Small 5 (2009) 795–799.
[14] S. Anaya, B. Serrano, B. Herrero, A. Cervera, J. Baselga, Γ-alumina modification with long chain carboxylic acid surface nanocrystals for biocompatible polysulfone nanocomposites, ACS Appl. Mater. Interfaces 6 (2014) 14460–14468.[15] L. Yu, Y. Zhang, B. Zhang, J. Liu, H. Zhang, C. Song, Preparation and characterization of HPEI-GO/PES ultrafiltration membrane with antifouling and antibacterial properties, J. Membr. Sci. 447 (2013) 452–462.
[16] J. Lee, H.-R. Chae, Y.J. Won, K. Lee, C.-H. Lee, H.H. Lee, I.-C. Kim, J. Lee, Graphene oxide nanoplatelets composite membrane with hydrophilic and antifouling properties for wastewater treatment, J. Membr. Sci. 448 (2013) 223–230.
[17] H.M. Hegab, A. ElMekawy, L. Zou, D. Mulcahy, C.P. Saint, M. Ginic-Markovic, The controversial antibacterial activity of graphene-based materials, Carbon N. Y. 105 (2016) 362–376.
[18] C.M. Santos, J. Mangadlao, F. Ahmed, A. Leon, R.C. Advincula, D.F. Rodrigues, Graphene nanocomposite for biomedical applications: fabrication, antimicrobial and cytotoxic investigations, Nanotechnology 23 (2012) 395101.
[19] Y.L.F. Musico, C.M. Santos, M.L.P. Dalida, D.F. Rodrigues, Surface modification of membrane filters using graphene and graphene oxide-based nanomaterials for bacterial inactivation and removal, ACS Sustain. Chem. Eng. 2 (2014) 1559–1565.
[20] J.D. Mangadlao, C.M. Santos, M.J.L. Felipe, A.C.C. de Leon, D.F. Rodrigues, R.C. Advincula, On the antibacterial mechanism of graphene oxide (GO) Langmuir–Blodgett films, Chem. Commun. 51 (2015) 2886–2889.
[21] I.E. Mejías Carpio, C.M. Santos, X. Wei, D.F. Rodrigues, Toxicity of a polymer–graphene oxide composite against bacterial planktonic cells, biofilms, and mammalian cells, Nanoscale 4 (2012) 4746.
[22] L. Yan, F. Zhao, S. Li, Z. Huc, Y. Zhao, Low-toxic and safe nanomaterials by surface-chemical design, carbon nanotubes, fullerenes, metallofullerenes, and graphenes, Nanoscale 3 (2011) 362–382.
[23] K.K. Yang, Behavior and toxicity of graphene and its functionalized derivatives in biological systems, Small 9 (2013) 1492–1503.
[24] A. Arora, G.W. Padua, Review: nanocomposites in food packaging, J. Food Sci. 75 (2010) 43–49.
[25] J.M. Bak, H. Lee, pH-tunable aqueous dispersion of graphene nanocomposites functionalized with poly(acrylic acid) brushes, Polym. (Guildf) 53 (2012) 4955–4960.
[26] J.M. Bak, T. Lee, E. Seo, Y. Lee, H.M. Jeong, B.-S. Kim, H. Lee, Thermoresponsive graphene nanosheets by functionalization with polymer brushes, Polym. (Guildf) 53 (2012) 316–323.
[27] L. Ren, X. Wang, S. Guo, T. Liu, Functionalization of thermally reduced graphene by in situ atom transfer radical polymerization, J. Nanopart. Res. 13 (2011) 6389–6396.
[28] Y. Li, B.C. Benicewicz, Functionalization of silica nanoparticles via the combination of surface-initiated RAFT polymerization and click reactions, Macromolecules 41 (2008) 7986–7992.
[29] Y. Yang, Y. Xie, L. Pang, M. Li, X. Song, J. Wen, H. Zhao, Preparation of reduced graphene oxide/poly(acrylamide) nanocomposite and its adsorption of Pb(II) and methylene blue, Langmuir 29 (2013) 10727–10736.
[30] H.H. Yang, "Click" preparation of CuPt nanorod-anchored graphene oxide as a catalyst in water, Small 8 (2012) 3161–3168.
[31] S. Rana, J.W. Cho, Functionalization of carbon nanotubes via Cu(I)-catalyzed Huisgen [3 + 2] cycloaddition "click chemistry", Nanoscale 2 (2010) 2550–2556.
[32] S. Sun, Y. Cao, J. Feng, P. Wu, Click chemistry as a route for the immobilization of well-defined polystyrene onto graphene sheets, J. Mater. Chem. 20 (2010) 5605.
[33] J. Han, C. Gao, Functionalization of carbon nanotubes and other nanocarbons by azide chemistry, Nano-Micro Lett. 2 (2010) 213–226.
[34] Y.Y. Liu, Cation-controlled aqueous dispersions of alginic-acid-wrapped multiwalled carbon nanotubes, Small 2 (2006) 874–878.
[35] X. Xu, Q. Luo, W. Lv, Y. Dong, Y. Lin, Q. Yang, A. Shen, D. Pang, J. Hu, J. Qin, Z. Li, Functionalization of graphene sheets by polyacetylene: convenient synthesis and enhanced emission, Macromol. Chem. Phys. 212 (2011) 768–773.
[36] H. He, C. Gao, General approach to individually dispersed, highly soluble, and conductive graphene nanosheets functionalized by nitrene chemistry, Chem. Mater 22 (2010) 5054–5064.
[37] T.A. Strom, E.P. Dillon, C.E. Hamilton, A.R. Barron, Nitrene addition to exfoliated graphene: a one-step route to highly functionalized graphene, Chem. Commun. (Camb) 46 (2010) 4097–4099.
[38] H.-X. Wang, K.-G. Zhou, Y.-L. Xie, J. Zeng, N.-N. Chai, J. Li, H.-L. Zhang, Photoactive graphene sheets prepared by "click" chemistry, Chem. Commun. (Camb) 47 (2011) 5747–5749.

[39] G. Yilmaz, H. Toiserkani, D.O. Demirkol, S. Sakarya, S. Timur, Y. Yagci, L. Torun, Modification of polysulfones by click chemistry: amphiphilic graft copolymers and their protein adsorption and cell adhesion properties, J. Polym. Sci. Part A Polym. Chem. 49 (2011) 110–117.

[40] A.B. Dongil, B. Bachiller-Baeza, A. Guerrero-Ruiz, I. Rodriguez-Ramos, Chemoselective hydrogenation of cinnamaldehyde: a comparison of the immobilization of Ru-phosphine complex on graphite oxide and on graphitic surfaces, J. Catal. 282 (2011) 299–309.

[41] N. Pantamas, C. Khonkeng, S. Krachodnok, A. Chaisena, Ecofriendly and simplified synthetic route for polysulfone-based solid-state alkaline electro-lyte membrane, Department of Chemistry and Center for Innovation in Chemistry, Fa, Am. J. Appl. Sci. 9 (2012) 1577–1582.

[42] A.M. G, P.R. Lewis, Biological Specimen Preparation for Transmission Electron Microscopy, 2014.

[43] S. Liu, T.H. Zeng, M. Hofmann, E. Burcombe, J. Wei, R. Jiang, J. Kong, Y. Chen, Antibacterial activity of graphite, graphite oxide, graphene oxide, and reduced graphene oxide: membrane and oxidative stress, ACS Nano 5 (2011) 6971–6980.

[44] C.M. Santos, M.C.R. Tria, R.A.M.V. Vergara, F. Ahmed, R.C. Advincula, D.F. Rodrigues, Antimicrobial graphene polymer (PVK-GO) nanocomposite films, Chem. Commun. (Camb) 47 (2011) 8892–8894.

[45] A. Warshawsky, N. Kahana, A. Deshe, H.E. Gottlieb, R. Arad-Yellin, Halomethylated polysulfone: reactive intermediates to neutral and ionic film-forming polymers, J. Polym. Sci. Part A Polym. Chem. 28 (1990) 2885–2905.

[46] A.C. Ferrari, Raman spectroscopy of graphene and graphite: disorder, electron-phonon coupling, doping and nonadiabatic effects, Solid State Commun. 143 (2007) 47–57.

[47] K.N. Kudin, B. Ozbas, H.C. Schniepp, R.K. Prud'homme, I.A. Aksay, R. Car, Raman spectra of graphite oxide and functionalized graphene sheets, Nano Lett. 8 (2008) 36–41.

[48] R. Saitoa, M. Hofmannb, G. Dresselhausc, A. Joriod, M.S. Dresselhausbe, Raman spectroscopy of graphene and carbon nanotubes, Adv. Phys. 60 (2011) 413–550.

[49] Y.-S. Ye, Y.-N. Chen, J.-S. Wang, J. Rick, Y.-J. Huang, F.-C. Chang, B.-J. Hwang, Versatile grafting approaches to functionalizing individually dispersed graphene nanosheets using RAFT polymerization and click chemistry, Chem. Mater. 24 (2012) 2987–2997.

[50] J. Qiu, et al., Hydrophilic modification of microporous polysulfone membrane via surface-initiated atom transfer radical polymerization of acrylamide, Appl. Surf. Sci. 256 (2010) 3274–3280.

[51] K. Haubner, J. Murawski, P. Olk, L.M. Eng, C. Ziegler, B. Adolphi, E. Jaehne, The route to functional graphene oxide, ChemPhysChem. 11 (2010) 2131–2139.

[52] J.F. Moulder, P.E. Stickle, P.E. Sobol, K.D. Bomben, Handbook of X-ray Photoelectron Spectroscopy, Perkin-Elmer Cor-poration, 1992.

[53] L.-H. Liu, G. Zorn, D.G. Castner, R. Solanki, M.M. Lerner, M. Yan, A simple and scalable route to wafer-size patterned graphene, J. Mater. Chem. 20 (2010) 5041–5046.

[54] S.C. Smith, D.F. Rodrigues, Carbon-based nanomaterials for removal of chemical and biological contaminants from water: a review of mechanisms and applications, Carbon N. Y. 91 (2015) 122–143.

[55] Y. Zhang, S.F. Ali, E. Dervishi, Y. Xu, Z. Li, D. Casciano, A.S. Biris, Cytotoxicity effects of graphene and single-wall carbon nanotubes in neural phaeochromocytoma-derived pc12 cells, ACS Nano 4 (2010) 3181–3186.

[56] S. Ramakrishna, J. Mayer, E. Wintermantel, K.W. Leong, Biomedical applications of polymer-composite materials: a review, Compos. Sci. Technol. 61 (2001) 1189–1224.

[57] E. Celik, H. Park, H. Choi, H. Choi, Carbon nanotube blended polyethersulfone membranes for fouling control in water treatment, Water Res. 45 (2011) 274–282.